Validation of Real-Time Solar Irradiance Simulations over Kuwait Using WRF-Solar

Christian A. Gueymard[1] and Pedro A. Jimenez[2]

[1] Solar Consulting Services, Colebrook, NH (USA)

[2] National Center for Atmospheric Research, Boulder, CO (USA)

Abstract

The performance of the WRF-Solar© mesoscale model is evaluated in the desert environment of Kuwait's Shagaya Park, where various solar technologies are being deployed. WRF-Solar is configured with one large domain (D1) covering the Arabian Peninsula and a nested domain (D2) centered on Kuwait. The daily simulations focus on the day-ahead forecast, and span the whole year of 2017. The initial and boundary conditions are provided by the GFS analysis, and the aerosol information is imported from NASA's GEOS-5 analysis. WRF-Solar predicts an absence of cloudiness 80% of the time. During such periods, the aerosol optical depth (AOD) predicted by GEOS-5 is found biased compared to local AERONET observations, which negatively impacts the performance of irradiance predictions, particularly for direct irradiance and under high-AOD situations. The impact of the horizontal grid spacing is evaluated. During cloudless conditions, the forecasts obtained for D1 and D2 are found practically identical. During cloudy conditions, however, mixed results are obtained. D2's results do offer improvement over those from D1 in some cases (depending on type of cloudiness), but not in general. By comparison with high-quality local irradiance observations, it is found that many situations evaluated as cloudless by WRF-Solar are actually cloudy, or vice versa. The performance of the Fast All-sky Radiation model for Solar applications (FARMS), now incorporated into WRF-Solar, is evaluated here in a desert environment for the first time and compared to that of the more established Rapid Radiative Transfer Model for GCMs (RRTMG). The two models satisfactorily agree under cloudless conditions, but not always under cloudy conditions. Depending on cloud conditions, one or the other might be closer to observations. In general, neither model is able to forecast the variations of direct irradiance with acceptable accuracy under clouds, which can be a concern for concentrating solar applications.

Keywords: WRF-Solar, aerosols, solar irradiance, Kuwait, forecast, GEOS-5, AERONET

1. Introduction

The Kuwait Institute for Scientific Research (KISR) oversees the development of various sources of renewable energy in Shagaya, Kuwait, a remote desert site. This is part of a national initiative to develop alternative energy sources and limit the internal consumption of oil for electricity production. Current installations in service or in construction at Shagaya amount to 70 MW, including solar photovoltaics (PV), concentrating solar power (CSP), and wind turbines. More installations (1.5 GW) are scheduled in the near future, so that a significant fraction of the electricity production in Kuwait will soon be provided by *variable* sources. To avoid problems due to grid instability or brownouts, KISR is now cooperating with the National Center for Atmospheric Research (NCAR) and Solar Consulting Services (SCS) to develop the necessary capabilities to obtain forecasts of the power production. For that purpose, NCAR is developing new forecasting tools based on previous experience (Haupt and Kosovic, 2016; Haupt et al., 2018). These forecasting tools incorporate a number of components to efficiently forecast the resource (solar or wind) itself, and the power production. The forecast horizon is typically 15 min to 7 days.

In the case of solar applications, the main components are a mesoscale numerical weather prediction (NWP) model, an advanced machine-learning toolkit, and a powerful blending integrator, with external information about the power plant's physical characteristics (Haupt et al., 2018). The present contribution proposes a preliminary investigation into the accuracy of irradiance predictions using a solar-enhanced version of the Weather Research and Forecasting (WRF-Solar©) mesoscale model (Jimenez et al., 2016a, 2016b; Powers et al., 2017) over Kuwait. WRF, and more recently WRF-Solar, have been used in a considerable number of studies related to the solar (or wind) forecasts in the context of renewable energy applications (Diagne et al., 2014; Eissa et al., 2018; Lara-Fanego et al., 2012a; Lee et al. 2017; Liu et al., 2016; Mukkavilli et al., 2018; Pierro et al., 2015), and to the as-

doi:10.18086/eurosun2018.09.14 Available at http://proceedings.ises.org

sessment of the solar resource (Almeida et al., 2015; Fountoukis et al., 2018; Ruiz-Arias et al., 2013; 2015). Here, some new features of WRF-Solar are investigated. Additionally, the performance of the model is assessed by comparing its predictions to actual high-quality irradiance measurements, while testing the role of the spatial resolution assigned to the study domain. The latter issue is important in general because NWP simulations require a lot of computer resources, which increase as an inverse quadratic function of the grid cell size. Hence, one objective of this study is to investigate whether a fine spatial resolution (such as 3 km) is necessary to improve irradiance forecasts, compared to a cruder resolution (such as 9 km).

In the particular case of Kuwait, cloudy periods are irregular and somewhat seasonal, but hazy situations caused by episodes of high dust aerosol loads are frequent. Such situations result in significant attenuation of the solar resource, and ultimately on soiling of all solar systems, which decreases their efficiency. An objective of this study is to investigate the impact of external sources of aerosol forecasts on the prediction of the irradiance incident on solar systems. The related soiling issue is beyond the scope of this contribution, however.

2. Mesoscale modeling with WRF-Solar

Irradiance predictions for a whole year (2017) are performed with the WRF-Solar mesoscale model, version 3.9.1.1 (Jimenez et al., 2016a). The Fast All-sky Radiation model for Solar applications (FARMS) model (Xie et al., 2016) was recently added to WRF-Solar as a new option. After a large number of tests, various issues (which will be described in a separate report) were found with its implementation. Version 3.9.1.1 introduced appropriate fixes to these issues, although a few small additional fixes can be expected in the near future, based on the results of the present study in particular.

For solar forecasting using any version of WRF, it is usual to consider a number of nested domains. For instance, Lara-Fanego et al. (2012b) and Kim et al. (2017) used four nested domains to simulate direct normal irradiance (DNI) over southern Spain and South Korea, respectively. Similarly, Lara-Fanego et al. (2012a) used three nested domains to simulate DNI and global horizontal irradiance (GHI) over the Andalusia region of Spain. Interestingly, the results of Lara-Fanego et al. (2012b) showed that the forecasting performance improved only imperceptibly between the third domain at 3-km resolution and the fourth (and innermost) domain at 1-km resolution. Partially based on these results, the experiment conducted here has been simplified to the point of using only two domains: An outer domain (D1) with 9-km spatial resolution, and an inner domain (D2) at 3-km resolution. Both domains use 45 layers in the vertical with the model lid at 100 hPa.

A number of processes are parameterized. Cloud microphysics is based on Thompson et al. (2008), whereas the cumulus parameterization (only active in D1) follows Grell and Freitas (2014). The Mellor–Yamada–Nakanishi–Niino (MYNN) planetary boundary layer parameterization (Nakanishi and Niino, 2006) and the revised Fifth-Generation Mesoscale Model (MM5) surface layer formulation (Jimenez et al., 2012) are used in the two domains. The unified National Centers for Environmental Prediction–Oregon State University–Air Force–Hydrologic Research Laboratory (NOAH) land surface model is adopted (Tewari et al., 2004). The parameterization of the aerosol interactions with radiation follows Ruiz-Arias et al. (2014), whereas the longwave radiation is parameterized using RRTM (Mlawer et al., 1997). Two shortwave radiation parameterizations, RRTMG and FARMS, are evaluated and more details are provided below.

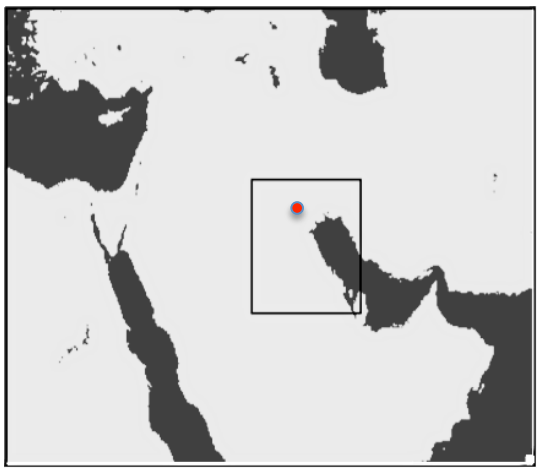

Fig. 1: Land mask of the region covered by the two domains. The inner domain, at 3-km resolution, covers Kuwait. The red dot indicates the Shagaya Park.

For the present investigation, separate forecasts are obtained over two separate domains. One large outer domain (D1) covers the Arabian Peninsula with a 9-km resolution and a nested inner 3-km-resolution domain (D2) is centered on Kuwait (Fig. 1). Each day, the model is initialized at 00 UTC and is run for 48 hours to focus on the day-ahead forecast. Hence, 365 daily simulations are performed here with WRF-Solar. Each domain provides independent irradiance simulations, which are helpful to quantify sensitivities of the predictions to the grid spacing. One important question being addressed here is how the 9-km and 3-km simulations compare over Kuwait. The importance of this question stems from the fact that WRF simulations over an inner (high-resolution) domain are computationally intensive. If this additional computational load were found not to yield significant performance improvements in the forecasts, a faster, low-resolution single-domain simulation might become sufficient.

Solar irradiance predictions are known to be sensitive to the radiative transfer model being used. This is true in the case of predictions related to the past (Fouquart et al., 1991), even when restricted to clear-sky situations (Gueymard and Ruiz-Arias, 2015). This is also true for DNI or GHI forecasts from NWP simulations (Montornès et al., 2015; Ronzio et al., 2013; Zhong et al., 2016). For the present contribution, the performance of two radiative transfer algorithms is examined. The first one is the Rapid Radiative Transfer Model for GCMs, better known as RRTMG (Iacono et al., 2008; Mlawer et al., 2016), which is well established and has been a standard radiative transfer parameterization in WRF and other NWP systems for many years. Its parameterization is computationally demanding, however, and thus is not typically called every time step of the model. In the present WRF-Solar simulations, RRTMG is called every 5 minutes. In between these calls, the irradiance is kept constant at all atmospheric levels. The second radiative transfer algorithm is the Fast All-sky Radiation model for Solar applications (FARMS; Xie et al., 2016). Contrary to RRTMG, FARMS only provides *surface* irradiances, which allows for their fast calculation, and makes it possible to call FARMS at each time step of the WRF-Solar model. The time step is 30 s in the 9-km domain (i.e., 10 times during a 5-min interval), and 3 times finer in the 3-km domain. This rapid cycle is attractive for solar irradiance applications that demand high temporal resolution, such as short-term forecasting. The performance of FARMS coupled with the WRF-Solar model has not been investigated before, and hence constitutes one important goal here.

3. Sources of data

WRF-Solar being a regional NWP model, it requires the specification of initial and boundary conditions representing the atmospheric state. In the present case, these conditions are imposed from the Global Forecast System (GFS) analyses run by NOAA. These are available every six hours at 0.25°x0.25° spatial resolution. In addition, the aerosol optical depth (AOD) at 550 nm is imposed every hour from the aerosol analysis performed with NASA's Goddard Earth Observing System version 5 (GEOS-5) model, initially at ≈25-km resolution. GEOS-5 assimilates a number of actual aerosol observations, from either satellite platforms (e.g., NASA's Moderate Resolution Imaging Spectroradiometer, MODIS, or Multi-angle Imaging SpectroRadiometer, MISR) or surface measurements from NASA's Aerosol Robotic Network (AERONET). To the authors' knowledge, however, this assimilation does not use data from the two AERONET sites that exist in Kuwait. Since the latter type of observations has much lower uncertainty than those from satellites, it is possible that the aerosol information generated by GEOS-5 is biased over Kuwait. This is investigated further in Section 4.

WRF-Solar's predictions are compared here to irradiance measurements carried out at the Shagaya Park station in Kuwait (lat. 29.21°N, long. 47.06°E, elev. 242 m), which is part of the KISR radiometric network (Al-Rasheedi et al., 2014). Solar irradiance observations are done with a time resolution of 1 minute, and include separate measurements of direct normal irradiance (DNI), global horizontal irradiance (GHI), and diffuse horizontal irradiance (DIF) made with individual thermopile radiometers. Helpful redundancy is provided by a rotating shadowband irradiometer (RSI). A stringent maintenance program, including daily cleaning of all instruments, results in a very high quality of the whole dataset. In particular, the RSI and thermopile observations have been found in close agreement (Al-Rasheedi et al., 2018). A time series of the best possible values of DNI, GHI and DIF has been assembled since 2012, and is used here for validation purposes. Measurement uncertainty is estimated to be ≈2% for DNI and ≈4% for GHI under normal conditions, and somewhat higher during dust storm conditions due to rapid soiling (Gueymard and Myers, 2008). A sunphotometer has been added to the station in 2015, and has joined the AERONET network since then. This instrument provides the aerosol optical depth (AOD) at seven wavelengths, the Ångström exponent (AEX), and precipitable water (PW) approximately every 15 min whenever the sun is unobscured by clouds. If AOD, AEX and PW are known precisely (as with AERONET data), it is possible to evaluate the clear-sky irradiances with good accuracy for that moment, even under the very hazy conditions that can occur in Kuwait (Gueymard et al., 2017). Under cloudless conditions, AOD is the main atmospheric driver for

DNI, and has a lesser, but still significant, impact on GHI (Gueymard, 2012). To forecast these two quantities correctly, it is thus necessary to use appropriate AOD estimates. Three potential avenues are possible, but none is bias-free: (i) Use an AOD climatology (i.e., a fixed pre-calculated monthly value representative of the long-term mean aerosol conditions over the area); (ii) Use the AOD from the previous hour or day (assumed persistence); or (iii) Use an AOD forecast for the appropriate time horizon. The latter option is used here, as provided by GEOS-5 on an hourly basis.

4. Aerosol data accuracy

Considering the high frequency of cloudless conditions over Kuwait and the high impact of AOD on DNI and GHI, it is important to quantify the error propagation effects from AOD to the predicted surface irradiance, which can directly affect all forecasts. Figure 2 compares AOD values obtained from different sources during four clear or essentially clear days with (i) exceptionally low AOD (2017-12-11); (ii) low AOD (017-03-07 and 2017-03-17); and (iii) high AOD (2017-04-29). The AOD forecasts from GEOS-5 (which are used here as inputs to WRF-Solar) are compared to modeled data from NASA's MERRA-2—the reanalysis derived from GEOS-5—and to local ground observations from the Shagaya AERONET station. The significant and systematic difference between these results suggests that neither GEOS-5 nor MERRA-2 assimilates the observations from this AERONET station specifically. The present results corroborate a previous analysis (Gueymard et al., 2017), which indicated significant differences in AOD data between MERRA-2 predictions and the observations from two AERONET stations in Kuwait. At Shagaya, the absolute difference, ΔAOD, between the GEOS-5 forecasts and the AERONET ground truth is highly variable over time, but is rarely below 0.05. This bias can temporarily reach values larger than 1 when a dust event does reach the site but is not forecasted by GEOS-5, as in the 2017-04-29 case (Fig. 2, bottom right). The induced error in DNI can be evaluated from ΔAOD and the tabulated results provided by Gueymard (2012). For instance, for an air mass of ≈1.5 (or a sun zenith angle of ≈48°), it is found that the relative error in DNI is ≈10% for ΔAOD = 0.1. It is thus expected that systematic errors in DNI forecasts will result from the inadequacies in the AOD input that are documented here. The impact on GHI, however, can be expected to be 3–4 times less (Gueymard, 2012), due to compensation effects between the direct and diffuse components.

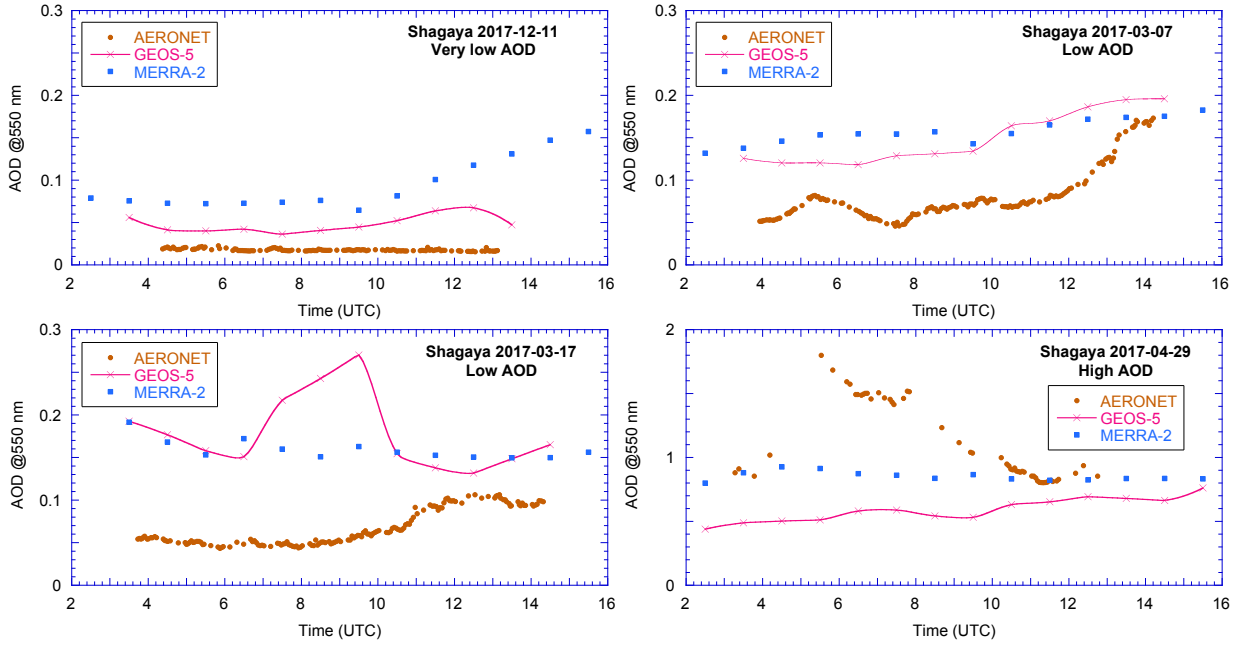

Fig. 2: Temporal variation of AOD at 550 nm at Shagaya during four cloudless (or nearly cloudless) days, as obtained from three sources: local AERONET observations, GEOS-5 forecasts, and MERRA-2 reanalysis. Note the different scale of the Y-axis in the high-AOD case (bottom right plot).

5. Simulation results

5.1. Cloudless conditions

Under cloudless conditions, the accuracy of WRF-Solar simulations is expected to depend mostly on that of the AOD inputs, per the discussion above. In this section, "cloudless conditions" are defined from the standpoint of WRF-Solar, i.e., whenever the forecasted total cloud liquid water path (CLW) is zero. During the daytime periods

of 2017, such conditions occurred 80.2% of the time. It is found that the irradiance forecasts for domains D1 and D2 are almost identical (the relative deviations in either DNI or GHI are within 1% on average), as could be expected considering that the footprint of either domain is much smaller than the spatial resolution of the AOD data from GEOS-5, and that the terrain is flat and homogenous around Shagaya.

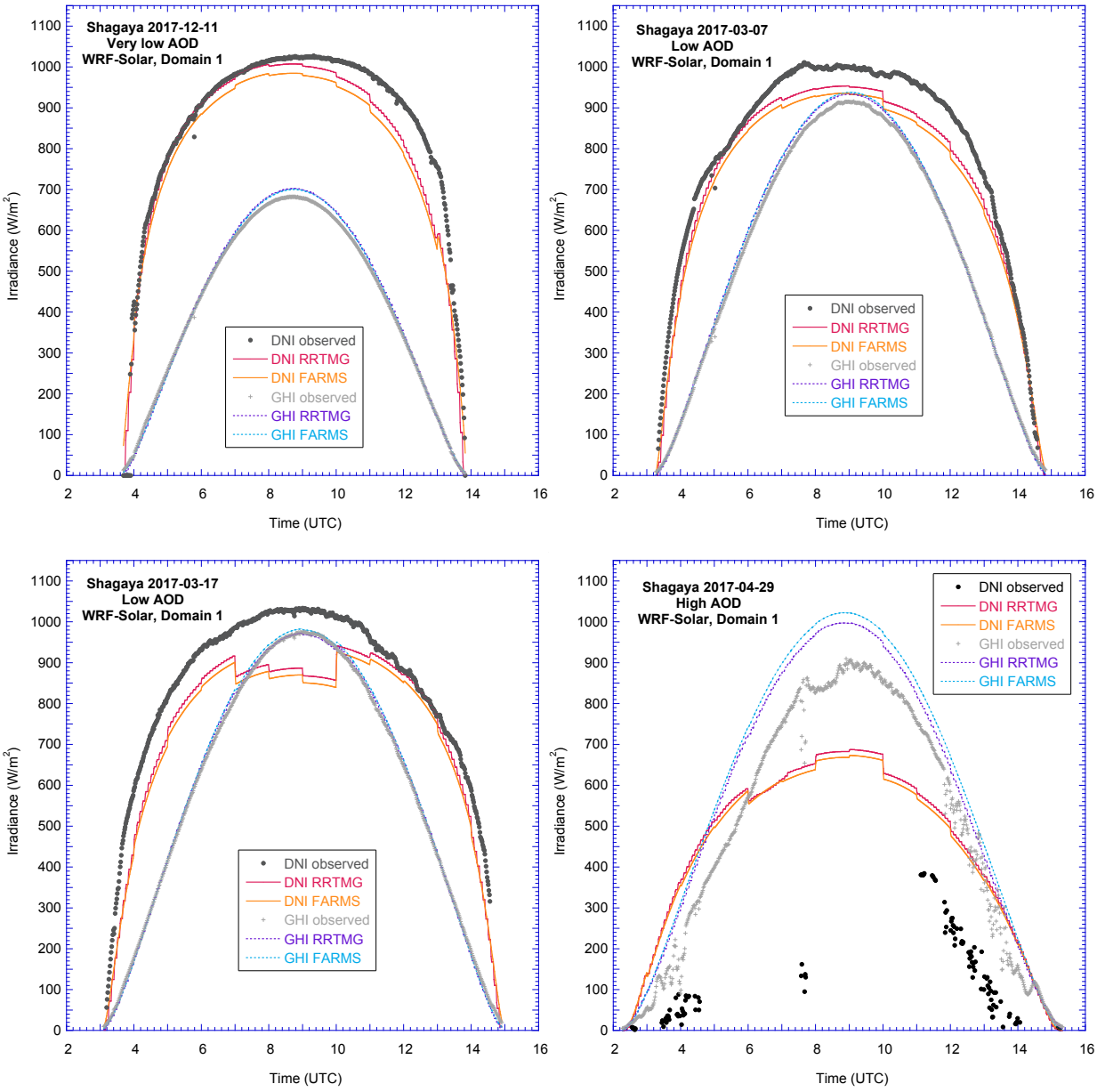

Fig. 3: Temporal variation of direct normal (DNI) and global horizontal (GHI) irradiance at Shagaya during the four cloudless (or nearly cloudless) days depicted in Fig. 2, as obtained from two radiative transfer models in WRF-Solar: RRTMG and FARMS, comparatively to local observations. The DNI observations that have been flagged during the quality control step are not shown. Most deviations between the modeled and measured values are caused by biased AOD inputs to the models.

Figure 3 shows the WRF-Solar forecasts for the same four days as in Fig. 2, based on the results from D1 at 9-km resolution. It can be observed that:

- DNI's predictions from RRTMG and FARMS quite systematically differ by ≈2%—a difference comparable to the experimental uncertainty in magnitude, and apparently caused by algorithmic variations—whereas their GHI predictions are almost identical, except under high-AOD circumstances.
- The DNI predictions tend to be too low compared to observations, as a direct consequence of GEOS-5's AOD being too high (Fig. 2).
- There are distinct discontinuities, or "steps", in the DNI results, which are caused by abrupt change in AOD data from one hour to the next (since no temporal interpolation is used).
- During the high-AOD event (2017-04-29), both DNI and GHI are considerably overestimated during most of the day.

- GHI predictions are only slightly higher than observations during the very low AOD event (top left) and the first low AOD event (top right), but are in good agreement with the observations during the second low AOD event (bottom left).

Based on these examples, it can be concluded that the slight DNI prediction difference between RRTMG and FARMS is usually small in comparison to the systematic misprediction caused by the imperfect AOD inputs. Scatterplots comparing DNI and GHI forecasts from RRTMG simulations over D1 are compared to their measured counterpart in Fig. 4. The plots are clearly not symmetric, with many points scattered on the left side of the diagonal. Those data points of lower-than-expected irradiance actually correspond to real-world cloudy situations that are misdiagnosed as "cloudless" by WRF-Solar. This issue translates into a tendency to overestimate DNI and GHI when the CLW forecast is zero. How this noise affects the relative performance of RRTMG and FARMS under truly cloudless conditions is still unclear. Considering all points shown in Fig. 4 and the usual statistics (mean bias deviation, MBD, and root mean square deviation, RMSD), the overall performance of FARMS appears slightly better than that of RRTMG for DNI: MBD is 3.1% and 0.7% for RRTMG and FARMS, whereas RMSD is 19.4% and 19.1%, respectively. For GHI, the opposite situation is found. MBD and RMSD are then 5.6% and 13.1% for RRTMG, and 7.7% and 14.6% for FARMS, respectively. Almost identical results are found over D2.

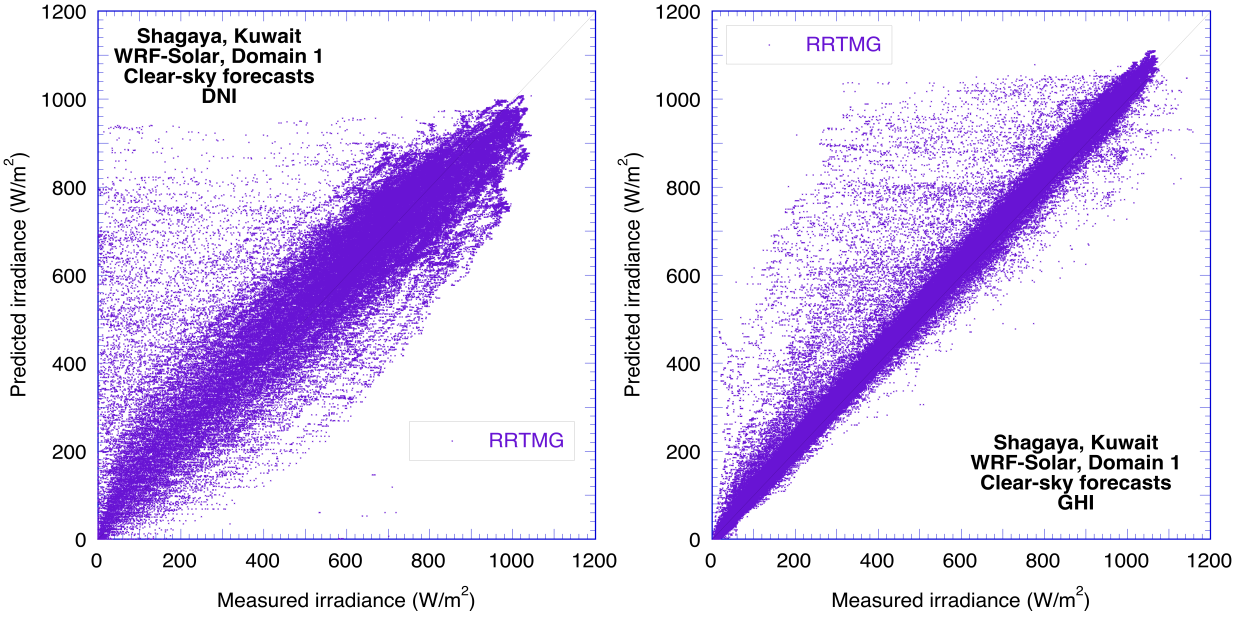

Fig. 4: Scatterplots of direct normal (DNI, left) and global horizontal (GHI, right) irradiance at Shagaya during 2017 as obtained with RRTMG over D1 during periods diagnosed as cloudless by WRF-Solar, comparatively to local observations.

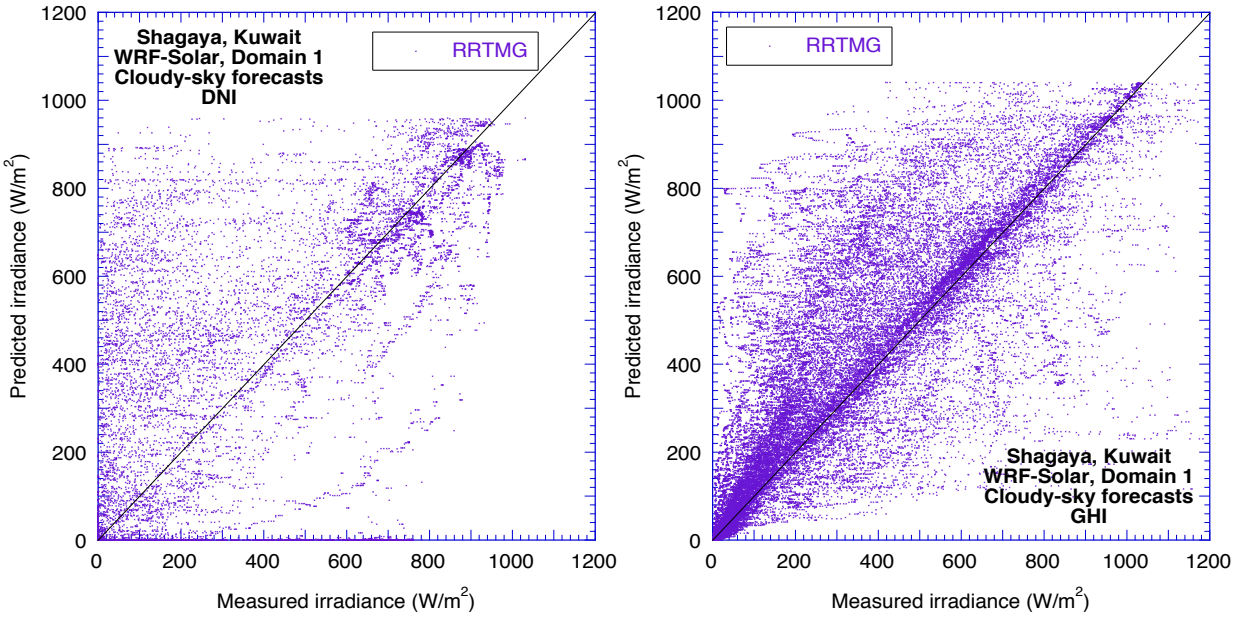

Fig. 5: Scatterplots of direct normal (DNI, left) and global horizontal (GHI, right) irradiance at Shagaya during 2017 as obtained with RRTMG over D1 during periods diagnosed as cloudy in either D1 or D2 by WRF-Solar, comparatively to local observations.

5.2. Cloudy conditions

When WRF-Solar does forecast cloudy periods (CLW > 0), the predictions of GHI and DNI differ more or less significantly from observations, depending on conditions and radiative model. Figure 5 shows scatterplots similar to those in Fig. 4, but for those periods diagnosed as cloudy by WRF-Solar in either D1 or D2, which represent 19.8% of the whole dataset. Note that, in about one seventh of these cases, the conditions are diagnosed cloudless by the D1 simulations and cloudy by D2, or vice versa. Compared to Fig. 4, the scatter is considerable here, particularly for DNI, as could be expected.

The large noise displayed in Fig. 5 can be explained by the misprediction of various characteristics of the cloud field. Even more noise is generated by FARMS, which however is less biased than RRTMG overall. To gain insight into the possible triggers of these circumstances, it is important to look into a number of cases with more scrutiny. For this analysis, four days are selected, during which the forecasts by RRTMG and FARMS differ substantially, and/or the simulations for D1 and D2 are remarkably different.

Figure 6a represents the GHI forecasts for a slightly cloudy day (2017-11-04), considering both radiative models and both domains. FARMS overestimates more than RRTMG until ≈10:30 UTC, then underestimates until 12:00 UTC. Between those two times, the average between RRTMG and FARMS would have provided the best estimate. For this specific day, the response from the two domains is similar with each model.

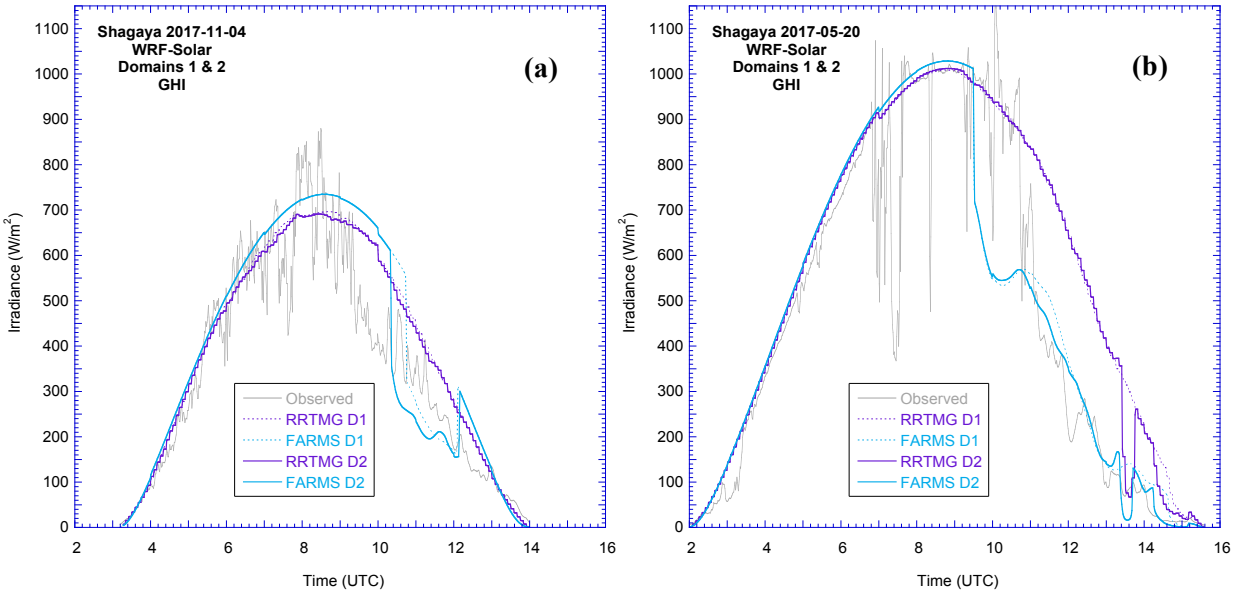

Fig. 6: Simulation of global horizontal irradiance at Shagaya during 2017-11-04 (a) and 2017-05-20 (b) as obtained with RRTMG and FARMS over both D1 and D2, comparatively to local observations.

Figure 6b is similar to Fig. 6a, but for 2017-05-20. In this case, cloudiness is more pronounced after 11:00 UTC. As before, the difference is small between the D1 and D2 results. Nevertheless, whereas RRTMG is closer to observations until 11:00 UTC, FARMS performs exceptionally well after that while RRTMG strongly overestimates.

In contrast with Fig. 6b, Fig. 7a shows results for D2 during 2017-04-16, during which scattered cloudiness conditions prevailed. The GHI predictions from FARMS then become unrealistically low, practically zero at times. The same kind of extreme FARMS underprediction occurs on 2017-05-05, for instance. The results for that day are shown in Fig, 7b, but only for RRTMG, which behaves much better. The contrast between the D1 and D2 simulations is obvious here, with the latter having a much more dynamic response to rapidly changing cloudiness. Note also the frequent cloud enhancement situations, which cannot currently be modeled by WRF-Solar. In particular, the observed GHI reached 1333 W/m^2 at 08:44 UTC, representing a 33% enhancement compared to the corresponding clear-sky value and 2% enhancement compared to the extraterrestrial value. Such circumstances are not unusual, and would be important to forecast because of the induced large ramps in power production and risks for the power electronics, such as inverters. More details on this issue are described in, e.g., Gueymard (2017). Although WRF-Solar may not be able to forecast the exact moments when these ramps occur, the fact that a highly variable GHI can be predicted using the D2 forecasts is in itself very valuable because it represents a clear alert of the risk of such ramps and/or cloud enhancement situations, based on which the solar system operator grid regulator can take appropriate decisions.

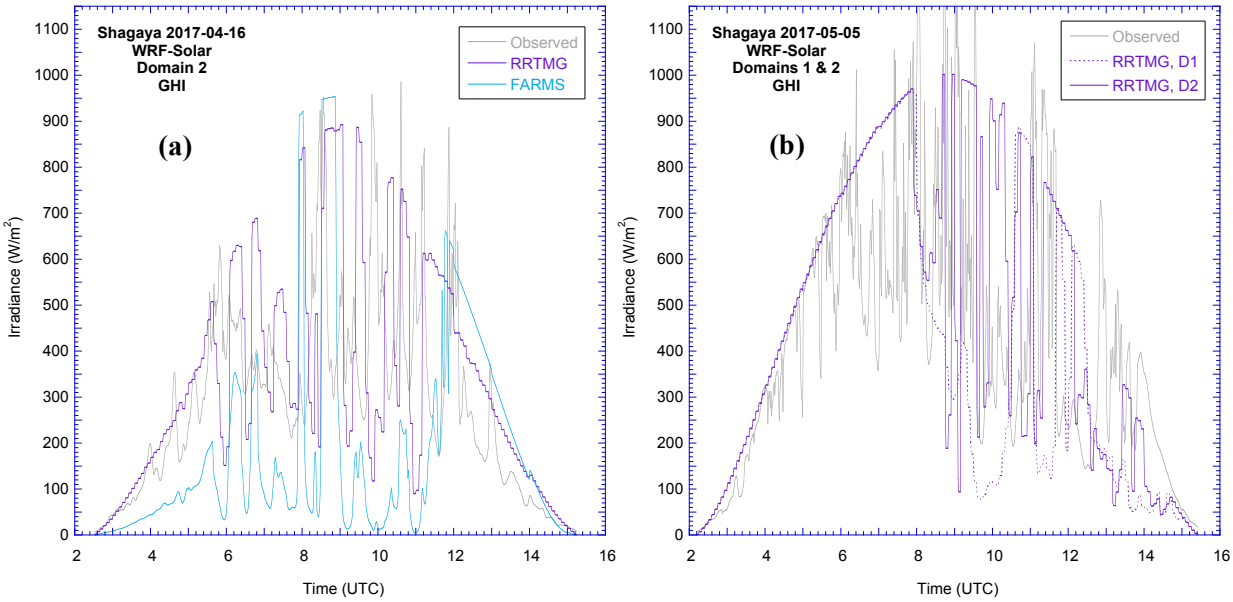

Fig. 7: Simulation of global horizontal irradiance at Shagaya during 2017-04-16 (a) and 2017-05-20 (b) as obtained with RRTMG and FARMS over both D1 and D2, comparatively to local observations.

5.3. Discussion

It is clear from the present results that RRTMG and FARMS tend to produce widely different predictions under various types of cloud conditions. It is anticipated that, in the near future, this can be exploited favorably through optimal combination of their results, thus leading to improved forecasts. Before this can be done, however, the FARMS implementation would first have to be corrected to eliminate its current shortcomings of, e.g. forecasting excessively low GHI under specific cloud conditions.

Tab. 1: Overall irradiance performance statistics for WRF-Solar forecasts at Shagaya, 2017 for domains D1 and D2, evaluated against observations (Obs.) of DNI and GHI. Clear conditions are selected based on WRF-Solar's diagnostic.

	DNI					GHI				
Statistic	Obs.	RRTMG-D1	FARMS-D1	RRTMG-D2	FARMS-D2	Obs.	RRTMG-D1	FARMS-D1	RRTMG-D2	FARMS-D2
CLEAR										
Mean (W/m²)	593.8	612.1	597.8	613.5	597.7	510.9	539.5	550.1	541.2	549.9
MBD (W/m²)		18.3	4.0	19.7	4.0		28.6	39.2	30.3	39.0
RMSD (W/m²)		115.4	113.7	115.5	113.8		67.1	74.4	68.1	74.4
MBD (%)		3.1	0.7	3.3	0.7		5.6	7.7	5.9	7.6
RMSD (%)		19.4	19.1	19.5	19.2		13.1	14.6	13.3	14.6
CLOUDY										
Mean (W/m²)	395.0	428.7	456.7	448.9	473.9	357.1	418.6	361.6	425.8	370.8
MBD (W/m²)		33.7	61.7	53.9	78.9		61.5	4.5	68.7	13.8
RMSD (W/m²)		273.0	284.0	259.2	272.4		187.0	207.0	189.4	204.0
MBD (%)		8.5	15.6	13.6	20.0		17.2	1.3	19.2	3.9
RMSD (%)		69.1	71.9	65.6	69.0		52.4	58.0	53.0	57.1
ALL										
Mean (W/m²)	576.0	595.7	585.2	598.8	586.7	481.5	516.3	514.0	519.1	515.7
MBD (W/m²)		19.7	9.2	22.7	10.7		34.9	32.5	37.7	34.2
RMSD (W/m²)		137.1	137.7	134.7	135.7		101.6	112.6	103.0	111.5
MBD (%)		3.4	1.6	3.9	1.8		7.2	6.8	7.8	7.1
RMSD (%)		23.8	23.9	23.4	23.6		21.1	23.4	21.4	23.2

Overall performance statistics are presented in Table 1, separately for the two irradiance components (DNI and GHI), the two domains (D1 and D2), the two radiative models (RRTMG and FARMS), and the three sky conditions as diagnosed by WRF-Solar (cloudless, cloudy in either D1 or D2, and all-sky conditions). Based on these simple statistics, and for the mostly cloudless conditions of Shagaya, the additional complexity of considering a high-resolution inner domain (D2) does not appear justified. This appears to be related to the "double penalty" issue, whereby the combination of observed-but-not-forecast and forecast-but-not-observed cases is more prevalent at high resolution than at low resolution (Ebert, 2008). Under clear (or nearly clear) conditions, the results for D2

are similar (but not better) than those for D1, since they are partly driven by inaccuracies in large-scale AOD data. Under cloudy situations, either the bias or variability (or both) in DNI and GHI tends to increase when considering D2 rather than D1, which seems counterproductive. Still, as mentioned in the previous section, a potentially useful (but currently unaccounted for) value of the D2 simulations might be the additional information about the expected rate of change of GHI and DNI. Further studies will look into a way to translate this qualitative information into a tangible performance indicator from a system operation perspective.

6. Conclusion

In this contribution, the WRF-Solar mesoscale model has been used to forecast the day-ahead surface solar irradiance at Shagaya, Kuwait. In this arid environment, cloudless conditions are predominant, while the aerosol optical depth (AOD) is highly variable and modulates the direct normal irradiance (DNI) and, to a lesser extent, the global horizontal irradiance (GHI).

To obtain simulations for the whole year 2017 with WRF-Solar, two nested domains are defined: An outer domain (D1) at 9-km resolution and an inner domain (D2) at 3-km resolution. The latter covers Kuwait entirely. The boundary conditions are provided by 6-hourly GFS forecasts. The aerosol field in D1 and D2 is determined by the hourly AOD analysis from NASA's GEOS-5 global model. By comparison with high-quality ground observations of AOD at the Shagaya AERONET station, it is found that the GEOS-5 AOD is most often biased, severely at times. A specific assessment of the forecasts obtained during those periods diagnosed as "cloudless" by WRF-Solar (representing ≈80% of all daytime periods) showed that the impact on the DNI forecasts is significant overall, and less significant on GHI. It can be inferred that the error propagation from the AOD inputs to the irradiance forecasts will affect concentrating solar thermal technologies more significantly than fixed-flat-plate photovoltaic (PV) generators, with intermediate effects on tracking PV systems. In parallel, it was found that a small, albeit sizeable, fraction of those periods that are found "cloudless" by WRF-Solar are actually cloudy, which tends to bias the performance results.

Under cloudless or nearly cloudless conditions, the performance of the D1 and D2 forecasts is very similar. For periods diagnosed as "cloudy" (representing ≈20% of all daytime situations overall), the D2 performance appears to degrade in comparison with that for D1. This counterintuitive result may have various causes, which are still being explored, but appear directly related to the "double penalty" issue. One apparent and possibly major cause is that, under rapidly changing scattered cloudiness, the D2 forecasts do correctly predict more temporal variability than the D1 forecasts—but with imprecise timing, which tends to increase the error in the forecast. Although the (costly) D2 forecasts for both DNI and GHI might appear unnecessary because of their lower performance, their main value might reside in the day-ahead prediction of rapidly variable irradiance. This ultimately could help system operators to prepare for strong ramps, cloud-enhancement effects, need for storage, or additional generation to avoid grid instability, etc.

The two radiative transfer, RRTMG vs. FARMS, used in parallel to evaluate the surface irradiance components returned similar predictions under cloudless conditions. Their ≈2% difference in DNI predictions is comparable to the experimental uncertainty. Under cloudy conditions, RRTMG performed somewhat better overall. Under some types of cloudiness situations, FARMS predicted unrealistically low GHI. This might be related to the current set of acceptable limits in cloud optical depth imposed on FARMS, which would need to be corrected in a future release of WRF-Solar. Under other cloud situations, though, FARMS performed better than RRTMG. Provided that any FARMS shortcoming in the model itself or its implementation can be addressed, it appears desirable to explore the development of an *optimal combination* of the two models' predictions. It is also anticipated that further post-processing, using soft-computing techniques applied to both RRTMG and FARMS results, will help improve forecasting accuracy for both GHI and DNI. Additionally, more research is needed to improve or appropriately correct the gridded AOD analyses that are required to obtain accurate DNI forecasts.

Acknowledgments

The authors thank Alaa Ismail, P.I. of the Shagaya Park station of AERONET and their staff. This work was funded by a research grant from the Kuwait Institute for Scientific Research. We particularly thank Dr. Majed Al-Rasheedi who oversees this project. The National Center for Atmospheric Research is sponsored by the U.S. National Science Foundation.

References

Almeida, M.P., Perpiñán, O., Narvarte, L., 2015. PV power forecast using a nonparametric PV model. Solar Energy 115, 354–368.

Al-Rasheedi, M., Gueymard, C.A., Ismail, A., Al-Hajraf, S., 2014. Solar resource assessment over Kuwait: validation of satellite-derived data and reanalysis modeling. Proc. ISES EuroSun 2014 Conf., Aix-les-Bains.

Al-Rasheedi, M., Gueymard, C.A., Ismail, A., Hussain, T., 2018. Comparison of two sensor technologies for solar irradiance measurement in a desert environment. Solar Energy 161, 194–206.

Diagne, M., David, M., Boland, J., Schmutz, N., Lauret, P., 2014. Post-processing of solar irradiance forecasts from WRF model at Reunion Island. Solar Energy 105, 99–108.

Ebert, E.E., 2008. Fuzzy verification of high-resolution gridded forecasts: a review and proposed framework. Meteorol. Appl. 15, 51–64.

Eissa, Y., Beegum, N.S., Gherboudj, I., Chaouch, N., Al Sudairi, J., Jones, R.K., Al Dobayan, N., Ghedira, H., 2018. Prediction of the day-ahead clear-sky downwelling surface solar irradiances using the REST2 model and WRF-CHIMERE simulations over the Arabian Peninsula. Solar Energy 162, 36–44.

Fountoukis, C., Martín-Pomares, L., Perez-Astudillo, D., Bachour, D., Gladich, I., 2018. Simulating global horizontal irradiance in the Arabian Peninsula: Sensitivity to explicit treatment of aerosols. Solar Energy 163, 347–355.

Fouquart, Y., Bonnel, B., Ramaswamy, V., 1991. Intercomparing shortwave radiation codes for climate studies. J. Geophys. Res. 96D, 8955–8968.

Grell, G.A., Freitas, S.R., 2014. A scale and aerosol aware stochastic convective parameterization for weather and air quality modeling, Atmos. Chem. Phys. 14, 5233–5250.

Gueymard, C.A., 2012. Temporal variability in direct and global irradiance at various time scales as affected by aerosols. Solar Energy 86, 3544–3553.

Gueymard, C.A., 2017. Cloud and albedo enhancement impacts on solar irradiance using high-frequency measurements from thermopile and photodiode radiometers. Part 1: Impacts on global horizontal irradiance. Solar Energy 153, 755–765.

Gueymard, C.A., Al-Rasheedi, M., Ismail, A., Hussain, T., 2017. Long-term variability of aerosol optical depth, dust episodes, and direct normal irradiance over Kuwait for CSP applications. Proc. ISES Solar World Congress, Abu Dhabi, UAE.

Gueymard, C.A., Myers, D.R., 2008. Solar radiation measurement: progress in radiometry for improved modeling. In: Badescu, V. (Ed.), Modeling Solar Radiation at the Earth Surface. Springer, pp. 1–27.

Gueymard, C.A., Ruiz-Arias, J.A., 2015. Validation of direct normal irradiance predictions under arid conditions: A review of radiative models and their turbidity-dependent performance. Renewable and Sustainable Energy Reviews 45, 379–396.

Haupt, S.E., Kosovic, B., 2016. Variable generation power forecasting as a big data problem. IEEE Transactions on Sustainable Energy 8, 725–732.

Haupt, S.E., Kosovic, B., Jensen, T., Lazo, J.K., Lee, J.A., Jimenez, P.A., Cowie, J., Wiener, G., McCandless, T.C., Rogers, M., Miller, S., Sengupta, M., Xie, Y., Hinkelman, L., Kalb, P., Heiser, J., 2018. Building the Sun4Cast system: Improvements in solar power forecasting. Bull. Amer Met. Soc. 99, 121-135.

Iacono, M.J., Delamere, J.S., Mlawer, E.J., Shephard, M.W., Clough, S.A., Collins, W.D., 2008. Radiative forcing by long-lived greenhouse gases: Calculations with the AER radiative transfer models. J. Geophys. Res. 113, D13103.

Jimenez, P.A., Dudhia, J., Gonzalez–Rouco, J.F., Navarro, J., Montavez, J.P., and Garcia–Bustamante, E., 2012. A revised scheme for the WRF surface layer formulation. Mon. Wea. Rev. 140**,** 898–918.

Jimenez, P.A., Hacker, J.P., Dudhia, J., Haupt, S.E., Ruiz-Arias, J.A., Gueymard, C.A., Thompson, G., Eidhammer, T., Deng, A., 2016a. WRF-Solar: description and clear-sky assessment of an augmented NWP model for solar power prediction. Bull. Am. Meteorol. Soc. 97, 1249–1264.

Jimenez, P.A., Alessandrini, S., Haupt, S.E., Deng. A., Kosovic, B., Lee, J.A., Delle Monache, L., 2016b. The role

of unresolved clouds on short-range global horizontal irradiance predictability. Mon. Wea. Rev. 144, 3099–3107.

Kim, J-Y., Yun, C-Y., Kim, C.K., Kang, Y-H., Kim, H-G, Lee, S-N., Kim, S-Y., 2017. Evaluation of WRF model-derived direct irradiance for solar thermal resource assessment over South Korea. AIP Conf. Proc. 1850, 140013; doi: 10.1063/1.4984521.

Lara-Fanego, V., Ruiz-Arias, J.A., Pozo-Vázquez, D., Santos-Alamillos, F.J., Tovar-Pescador, J., 2012a. Evaluation of the WRF model solar irradiance forecasts in Andalusia (southern Spain). Solar Energy 86, 2200–2217.

Lara-Fanego, V., Ruiz-Arias, J.A., Pozo-Vázquez, D., Gueymard, C.A., Tovar-Pescador, J., 2012b. Evaluation of DNI forecast based on the WRF mesoscale atmospheric model for CPV applications. AIP Conf. Proc. 1477, 317, doi: 10.1063/1.4753895.

Lee, J.A., Haupt, S.E., Jimenez, P.A., Rogers, M.A., Miller, S.D., McCandles, T., 2017. Solar irradiance nowcasting case studies near Sacramento. J. Appl. Meteorol. Climatol. 56, 85–108.

Liu, Y., Shimada, S., Yoshino, J., Kobayashi, T., Miwa, Y., Furuta, K., 2016. Ensemble forecasting of solar irradiance by applying a mesoscale meteorological model. Solar Energy 136, 597–605.

Mlawer, E.J., Iacono, M.J., Pincus, R., Barker, H.W., Oreopoulos, L., Mitchell, D.L., 2016. Contributions of the ARM Program to radiative transfer modeling for climate and weather applications. AMS Meteorological Monographs 57, 15.1–15.19.

Mlawer, E. J., Taubman, S.J., Brown, P.D., Iacono, M.J., Clough, S.A., 1997. Radiative transfer for inhomogeneous atmospheres: RRTM, a validated correlated–k model for the longwave. J. Geophys. Res. 102D, 16663–16682.

Montornès, A., Codina, B., Zack, J.W., 2015. A discussion about the role of shortwave schemes on real WRF-ARW simulations. Two case studies: cloudless and cloudy sky. Tethys 12, 13–31.

Mukkavilli, S.K., Prasad, A.A., Taylor, R.A. Troccoli, A., Kay, M.J., 2018. Mesoscale simulations of Australian direct normal irradiance, featuring an extreme dust event. J. Appl. Meteorol. Climatol. 57, 493–515.

Nakanishi, M., Niino, H., 2006. An improved Mellor–Yamada level 3 model: its numerical stability and application to a regional prediction of advecting fog. Bound. Layer Meteor. 119, 397–407.

Pierro, M., Bucci, F., Cornaro, C., Maggioni, E., Perotto, A., Pravettoni, M., Spada, F., 2015. Model output statistics cascade to improve day ahead solar irradiance forecast. Solar Energy 117, 99–113.

Powers, J.G., et al., 2017. The Weather Research and Forecasting model: overview, system efforts, and future directions. Bull. Amer. Meteor. Soc. 98, 1717–1737.

Ronzio, D.A., Collino, E., Bonelli, P., 2013. A survey on different radiative and cloud schemes for the solar radiation modeling. Solar Energy 98, 153–166.

Ruiz-Arias, J.A., Dudhia, J., Santos-Alamillos, F.J., Pozo-Vázquez1, D., 2013. Surface clear-sky shortwave radiative closure intercomparisons in the Weather Research and Forecasting model. J. Geophys. Res. 118D, 9901–9913.

Ruiz-Arias, J.A., Dudhia, J., Gueymard, C.A., 2014. A simple parameterization of the short-wave aerosol optical properties for surface direct and diffuse irradiances assessment in a numerical weather prediction model. Geosci. Model. Dev. 7, 1159–1174.

Ruiz-Arias, J.A., Quesada-Ruiz, S., Fernández, E.F., Gueymard, C.A., 2015. Optimal combination of gridded and ground-observed solar radiation data for regional solar resource assessment, Solar Energy 112, 411–424.

Tewari, M., Chen, F., Wang, W., Dudhia, J., LeMone, M.A., Mitchell, K., Ek, M., Gayno, G., Wegiel, J., Cuenca, R.H., 2004. Implementation and verification of the unified NOAH land surface model in the WRF model. *20th conference on weather analysis and forecasting/16th conference on numerical weather prediction*, pp. 11–15.

Thompson, G., Field, P.R., Rasmussen, R.M., Hall, W.D., 2008. Explicit forecasts of winter precipitation using an improved bulk microphysics scheme. Part II: Implementation of a new snow parameterization. Mon. Wea. Rev. 136**,** 5095–5115.

Xie, Y., Sengupta, M., Dudhia, J., 2016. A Fast All-sky Radiation Model for Solar applications (FARMS): Algorithm and performance evaluation. Solar Energy 135, 435–445.

Zhong, X., Ruiz-Arias, J.A., Kleissl. J., Dissecting surface clear sky irradiance bias in numerical weather prediction: Application and corrections to the New Goddard Shortwave Scheme. Solar Energy 132, 103–113.